# CHAPTER 54
# COOLING ELECTRONIC EQUIPMENT

**Allan Kraus**
**Allan D. Kraus Associates**
**Aurora, Ohio**



## 54.1 THERMAL MODELING

### 54.1.1 Introduction

To determine the temperature differences encountered in the flow of heat within electronic systems, it is necessary to recognize the relevant heat transfer mechanisms and their governing relations. In a typical system, heat removal from the active regions of the microcircuit(s) or chip(s) may require the use of several mechanisms, some operating in series and others in parallel, to transport the generated heat to the coolant or ultimate heat sink. Practitioners of the thermal arts and sciences generally deal with four basic thermal transport modes: conduction, convection, phase change, and radiation.

### 54.1.2 Conduction Heat Transfer

#### One-Dimensional Conduction

Steady thermal transport through solids is governed by the Fourier equation, which, in one-dimensional form, is expressible as

$$q = -kA\frac{dT}{dx} \quad \text{(W)} \tag{54.1}$$

where $q$ is the heat flow, $k$ is the thermal conductivity of the medium, $A$ is the cross-sectional area for the heat flow, and $dT/dx$ is the temperature gradient. Here, heat flow produced by a negative temperature gradient is considered positive. This convention requires the insertion of the minus sign in Eq. (54.1) to assure a positive heat flow, $q$. The temperature difference resulting from the steady state diffusion of heat is thus related to the thermal conductivity of the material, the cross-sectional area and the path length, $L$, according to

$$(T_1 - T_2)_{cd} = q\frac{L}{kA} \quad \text{(K)} \tag{54.2}$$

*Mechanical Engineers' Handbook,* 2nd ed., Edited by Myer Kutz.
ISBN 0-471-13007-9 

The form of Eq. (54.2) suggests that, by analogy to Ohm's Law governing electrical current flow through a resistance, it is possible to define a thermal resistance for conduction, $R_{cd}$, as

$$R_{cd} \equiv \frac{(T_1 - T_2)}{q} = \frac{L}{kA} \tag{54.3}$$

### One-Dimensional Conduction with Internal Heat Generation

Situations in which a solid experiences internal heat generation, such as that produced by the flow of an electric current, give rise to more complex governing equations and require greater care in obtaining the appropriate temperature differences. The axial temperature variation in a slim, internally heated conductor whose edges (ends) are held at a temperature $T_o$ is found to equal

$$T = T_o + q_g \frac{L^2}{2k}\left[\left(\frac{x}{L}\right) - \left(\frac{x}{L}\right)^2\right]$$

When the volumetic heat generation rate, $q_g$, in $W/m^3$ is uniform throughout, the peak temperature is developed at the center of the solid and is given by

$$T_{max} = T_o + q_g \frac{L^2}{8k} \quad (K) \tag{54.4}$$

Alternatively, because $q_g$ is the volumetric heat generation, $q_g = q/LW\delta$, the center–edge temperature difference can be expressed as

$$T_{max} - T_o = q \frac{L^2}{8kLW\delta} = q \frac{L}{8kA} \tag{54.5}$$

where the cross-sectional area, $A$, is the product of the width, $W$, and the thickness, $\delta$. An examination of Eq. (54.5) reveals that the thermal resistance of a conductor with a distributed heat input is only one quarter that of a structure in which all of the heat is generated at the center.

### Spreading Resistance

In chip packages that provide for lateral spreading of the heat generated in the chip, the increasing cross-sectional area for heat flow at successive"layers" below the chip reduces the internal thermal resistance. Unfortunately, however, there is an additional resistance associated with this lateral flow of heat. This, of course, must be taken into account in the determination of the overall chip package temperature difference.

For the circular and square geometries common in microelectronic applications, an engineering approximation for the spreading resistance for a small heat source on a thick substrate or heat spreader (required to be 3 to 5 times thicker than the square root of the heat source area) can be expressed as[1]

$$R_{sp} = \frac{0.475 - 0.62\epsilon + 0.13\epsilon^2}{k\sqrt{A_c}} \quad (K/W) \tag{54.6}$$

where $\epsilon$ is the ratio of the heat source area to the substrate area, $k$ is the thermal conductivity of the substrate, and $A_c$ is the area of the heat source.

For relatively thin layers on thicker substrates, such as encountered in the use of thin lead-frames, or heat spreaders interposed between the chip and substrate, Eq. (54.6) cannot provide an acceptable prediction of $R_{sp}$. Instead, use can be made of the numerical results plotted in Fig 54.1 to obtain the requisite value of the spreading resistance.

### Interface/Contact Resistance

Heat transfer across the interface between two solids is generally accompanied by a measurable temperature difference, which can be ascribed to a contact or interface thermal resistance. For perfectly adhering solids, geometrical differences in the crystal structure (lattice mismatch) can impede the flow of phonons and electrons across the interface, but this resistance is generally negligible in engineering design. However, when dealing with real interfaces, the asperities present on each of the surfaces, as shown in an artist's conception in Fig 54.2, limit actual contact between the two solids to a very small fraction of the apparent interface area. The flow of heat across the gap between two solids in nominal contact is thus seen to involve solid conduction in the areas of actual contact and fluid conduction across the "open" spaces. Radiation across the gap can be important in a vacuum environment or when the surface temperatures are high.

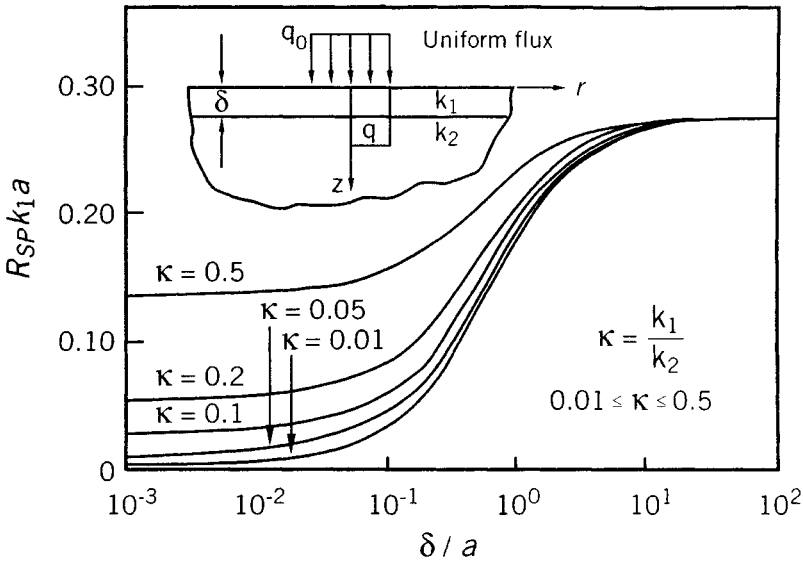


**Fig. 54.1** The thermal resistance for a circular heat source on a two layer substrate (from Ref. 2).

The heat transferred across an interface can be found by adding the effects of the solid–to–solid conduction and the conduction through the fluid and recognizing that the solid–to–solid conduction, in the contact zones, involves heat flowing sequentially through the two solids. With the total contact conductance, $h_{co}$, taken as the sum of the solid–to–solid conductance, $h_c$, and the gap conductance, $h_g$

$$h_{co} = h_c + h_g \qquad (W/m^2 \cdot K) \tag{54.7a}$$

the contact resistance based on the apparent contact area, $A_a$, may be defined as

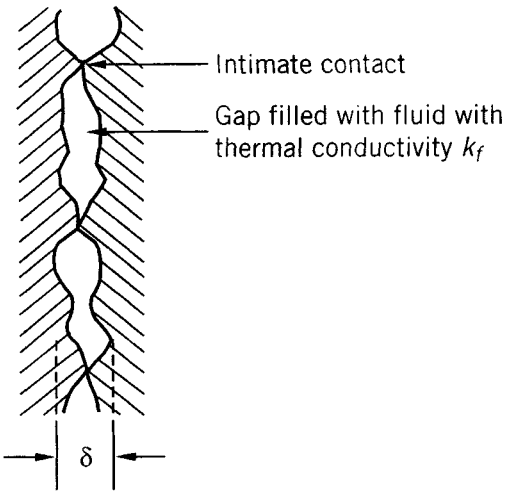


**Fig. 54.2** Physical contact between two nonideal surfaces.

$$R_{co} \equiv \frac{1}{h_{co}A_a} \qquad \text{(K/W)} \tag{54.7b}$$

In Eq. (54.7*a*), $h_c$ is given by

$$h_c = 54.25k_s\left(\frac{m}{\sigma}\right)\left(\frac{P}{H}\right)^{0.95} \tag{54.8a}$$

where $k_s$ is the harmonic mean thermal conductivity for the two solids with thermal conductivities, $k_1$ and $k_2$,

$$k_s = \frac{2k_1k_2}{k_1 + k_2} \qquad \text{(W/m} \cdot \text{K)}$$

$\sigma$ is the effective rms surface roughness developed from the surface roughnesses of the two materials, $\sigma_1$ and $\sigma_2$,

$$\sigma = \sqrt{\sigma_1^2 + \sigma_2^2} \qquad (\mu \cdot \text{m})$$

and $m$ is the effective absolute surface slope composed of the individual slopes of the two materials, $m_1$ and $m_2$,

$$m = \sqrt{m_1^2 + m_2^2}$$

where $P$ is the contact pressure and $H$ is the microhardness of the softer material, both in $N/m^2$. In the absence of detailed information, the $\sigma/m$ ratio can be taken equal to 5–9 microns for relatively smooth surfaces.[1,2]

In Eq. (54.7*a*), $h_g$ is given by

$$h_g = \frac{k_g}{Y + M} \tag{54.8b}$$

where $k_g$ is the thermal conductivity of the gap fluid, $Y$ is the distance between the mean planes (Fig. 54.2) given by

$$\frac{Y}{\sigma} = 54.185\left[-\ln\left(3.132\,\frac{P}{H}\right)\right]^{0.547}$$

and $M$ is a gas parameter used to account for rarefied gas effects

$$M = \alpha\beta\Lambda$$

where $\alpha$ is an accommodation parameter (approximately equal to 2.4 for air and clean metals), $\Lambda$ is the mean free path of the molecules (equal to approximately 0.06 $\mu$m for air at atmospheric pressure and 15°C), and $\beta$ is a fluid property parameter (equal to approximately 54.7 for air and other diatomic gases).

Equations (54.8*a*) and (54.8*b*) can be added and, in accordance with Eq. (54.7*b*), the contact resistance becomes

$$R_{co} \equiv \left\{\left[1.25k_s\left(\frac{m}{\sigma}\right)\left(\frac{P}{H}\right)^{0.95} + \frac{k_g}{Y + M}\right]A_a\right\}^{-1} \tag{54.9}$$

### 54.1.3 Convective Heat Transfer

#### The Heat Transfer Coefficient

Convective thermal transport from a surface to a fluid in motion can be related to the heat transfer coefficient, $h$, the surface–to–fluid temperature difference, and the "wetted" surface area, $S$, in the form

$$q = hS(T_s - T_{fl}) \qquad \text{(W)} \tag{54.10}$$

The differences between convection to a rapidly moving fluid, a slowly flowing or stagnant fluid,

as well as variations in the convective heat transfer rate among various fluids, are reflected in the values of $h$. For a particular geometry and flow regime, $h$ may be found from available empirical correlations and/or theoretical relations. Use of Eq. (54.10) makes it possible to define the convective thermal resistance as

$$R_{cv} \equiv \frac{1}{hS} \qquad (\text{K/W}) \tag{54.11}$$

### Dimensionless Parameters

Common dimensionless quantities that are used in the correlation of heat transfer data are the *Nusselt number,* Nu, which relates the convective heat transfer coefficient to the conduction in the fluid where the subscript, fl, pertains to a fluid property,

$$\text{Nu} \equiv \frac{h}{k_{fl}/L} = \frac{hL}{k_{fl}}$$

the *Prandtl number,* Pr, which is a fluid property parameter relating the diffusion of momentum to the conduction of heat,

$$\text{Pr} \equiv \frac{c_p \mu}{k_{fl}}$$

the *Grashof number,* Gr, which accounts for the bouyancy effect produced by the volumetric expansion of the fluid,

$$\text{Gr} \equiv \frac{\rho^2 \beta g L^3 \Delta T}{\mu^2}$$

and the *Reynolds number,* Re, which relates the momentum in the flow to the viscous dissipation,

$$\text{Re} \equiv \frac{\rho V L}{\mu}$$

### Natural Convection

In natural convection, fluid motion is induced by density differences resulting from temperature gradients in the fluid. The heat transfer coefficient for this regime can be related to the buoyancy and the thermal properties of the fluid through the *Rayleigh number,* which is the product of the Grashof and Prandtl numbers,

$$\text{Ra} = \frac{\rho^2 \beta g c_p}{\mu k_{fl}} L^3 \Delta T$$

where the fluid properties, $\rho$, $\beta$, $c_p$, $\mu$, and $k$, are evaluated at the fluid bulk temperature and $\Delta T$ is the temperature difference between the surface and the fluid.

Empirical correlations for the natural convection heat transfer coefficient generally take the form

$$h = C \left(\frac{k_{fl}}{L}\right) (\text{Ra})^n \qquad (\text{W/m}^2 \cdot \text{K}) \tag{54.12}$$

where $n$ is found to be approximately 0.25 for $10^3 < \text{Ra} < 10^9$, representing laminar flow, 0.33 for $10^9 < \text{Ra} < 10^{12}$, the region associated with the transition to turbulent flow, and 0.4 for $\text{Ra} > 10^{12}$, when strong turbulent flow prevails. The precise value of the correlating coefficient, $C$, depends on fluid, the geometry of the surface, and the Rayleigh number range. Nevertheless, for common plate, cylinder, and sphere configurations, it has been found to vary in the relatively narrow range of 0.45–0.65 for laminar flow and 0.11–0.15 for turbulent flow past the heated surface.[42]

Natural convection in vertical channels such as those formed by arrays of longitudinal fins is of major significance in the analysis and design of heat sinks and experiments for this configuration have been conducted and confirmed.[4,5]

These studies have revealed that the value of the Nusselt number lies between two extremes associated with the separation between the plates or the channel width. For wide spacing, the plates

appear to have little influence upon one another and the Nusselt number in this case achieves its *isolated plate limit*. On the other hand, for closely spaced plates or for relatively long channels, the fluid attains its *fully developed* value and the Nusselt number reaches its *fully developed limit*. Intermediate values of the Nusselt number can be obtained from a form of a correlating expression for smoothly varying processes and have been verified by detailed experimental and numerical studies.[19,20]

Thus, the correlation for the average value of $h$ along isothermal vertical placed separated by a spacing, $z$

$$h = \frac{k_{fl}}{z}\left[\frac{576}{(\mathrm{El})^2} + \frac{2.873}{(\mathrm{El})^{1/2}}\right]^{1/2} \tag{54.13}$$

where El is the *Elenbaas number*

$$\mathrm{El} \equiv \frac{\rho^2 \beta g c_p z^4 \Delta T}{\mu k_{fl} L}$$

and $\Delta T = T_s - T_{fl}$.

Several correlations for the coefficient of heat transfer in natural convection for various configurations are provided in Section 54.2.1.

### Forced Convection

For forced flow in long, or very narrow, parallel-plate channels, the heat transfer coefficient attains an asymptotic value (a fully developed limit), which for symmetrically heated channel surfaces is equal approximately to

$$h = \frac{4k_{fl}}{d_e} \qquad (\mathrm{W/m^2 \cdot K}) \tag{54.14}$$

where $d_e$ is the *hydraulic diameter* defined in terms of the flow area, $A$, and the wetted perimeter of the channel, $P_w$

$$d_e \equiv \frac{4A}{P_w}$$

Several correlations for the coefficient of heat transfer in forced convection for various configurations are provided in Section 54.2.2.

### Phase Change Heat Transfer

Boiling heat transfer displays a complex dependence on the temperature difference between the heated surface and the saturation temperature (boiling point) of the liquid. In nucleate boiling, the primary region of interest, the ebullient heat transfer rate can be approximated by a relation of the form

$$q_\phi = C_{sf} A (T_s - T_{\mathrm{sat}})^3 \qquad (\mathrm{W}) \tag{54.15}$$

where $C_{sf}$ is a function of the surface/fluid combination and various fluid properties. For comparison purposes, it is possible to define a boiling heat transfer coefficient, $h_\phi$,

$$h_\phi = C_{sf}(T_s - T_{\mathrm{sat}})^2 \qquad [\mathrm{W/m^2 \cdot K}]$$

which, however, will vary strongly with surface temperature.

### Finned Surfaces

A simplified discussion of finned surfaces is germane here and what now follows is not inconsistent with the subject matter contained Section 54.3.1. In the thermal design of electronic equipment, frequent use is made of finned or "extended" surfaces in the form of *heat sinks* or *coolers*. While such finning can substantially increase the surface area in contact with the coolant, resistance to heat flow in the fin reduces the average temperature of the exposed surface relative to the fin base. In the analysis of such finned surfaces, it is common to define a fin efficiency, $\eta$, equal to the ratio of the actual heat dissipated by the fin to the heat that would be dissipated if the fin possessed an infinite thermal conductivity. Using this approach, heat transferred from a fin or a fin structure can be expressed in the form

$$q_f = hS_f \eta (T_b - T_s) \qquad (\mathrm{W}) \tag{54.16}$$

where $T_b$ is the temperature at the base of the fin and where $T_s$ is the surrounding temperature and $q_f$ is the heat entering the base of the fin, which, in the steady state, is equal to the heat dissipated by the fin.

The thermal resistance of a finned surface is given by

$$R_f \equiv \frac{1}{hS_f\eta} \tag{54.17}$$

where $\eta$, the fin efficiency, is 0.627 for a thermally optimum rectangular cross section fin,[11]

### Flow Resistance

The transfer of heat to a flowing gas or liquid that is not undergoing a phase change results in an increase in the coolant temperature from an inlet temperature of $T_{in}$ to an outlet temperature of $T_{out}$, according to

$$q = mc_p(T_{out} - T_{in}) \qquad \text{(W)} \tag{54.18}$$

Based on this relation, it is possible to define an effective flow resistance, $R_{fl}$, as

$$R_{fl} \equiv \frac{1}{\dot{m}c_p} \qquad \text{(K/W)} \tag{54.19}$$

where $\dot{m}$ is in kg/sec.

### 54.1.4 Radiative Heat Transfer

Unlike conduction and convection, radiative heat transfer between two surfaces or between a surface and its surroundings is not linearly dependent on the temperature difference and is expressed instead as

$$q = \sigma S\mathfrak{F}(T_1^4 - T_2^4) \qquad \text{(W)} \tag{54.20}$$

where $\mathfrak{F}$ includes the effects of surface properties and geometry and $\sigma$ is the Stefan–Boltzman constant, $\sigma = 5.67 \times 10^{-8}$ W/m$^2 \cdot$ K$^4$. For modest temperature differences, this equation can be linearized to the form

$$q = h_r S(T_1 - T_2) \qquad \text{(W)} \tag{54.21}$$

where $h_r$ is the effective "radiation" heat transfer coefficient

$$h_r = \sigma\mathfrak{F}(T_1^2 + T_2^2)(T_1 + T_2) \qquad \text{(W/m}^2 \cdot \text{K)} \tag{54.22a}$$

and, for small $\Delta T = T_1 - T_2$, $h_r$ is approximately equal to

$$h_r = 4\sigma\mathfrak{F}(T_1T_2)^{3/2} \qquad \text{(W/m}^2 \cdot \text{K)} \tag{54.22b}$$

It is of interest to note that for temperature differences of the order of 10 K, the radiative heat transfer coefficient, $h_r$, for an ideal (or "black") surface in an absorbing environment is approximately equal to the heat transfer coefficient in natural convection of air.

Noting the form of Eq. (54.21), the radiation thermal resistance, analogous to the convective resistance, is seen to equal

$$R_r \equiv \frac{1}{h_rS} \qquad \text{(K/W)} \tag{54.23}$$

### Thermal Resistance Network

The expression of the governing heat transfer relations in the form of thermal resistances greatly simplifies the first-order thermal analysis of electronic systems. Following the established rules for resistance networks, thermal resistances that occur sequentially along a thermal path can be simply summed to establish the overall thermal resistance for that path. In similar fashion, the reciprocal of the effective overall resistance of several parallel heat transfer paths can be found by summing the reciprocals of the individual resistances. In refining the thermal design of an electronic system, prime attention should be devoted to reducing the largest resistances along a specified thermal path and/or providing parallel paths for heat removal from a critical area.

While the thermal resistances associated with various paths and thermal transport mechanisms constitute the "building blocks" in performing a detailed thermal analysis, they have also found

widespread application as "figures-of-merit" in evaluating and comparing the thermal efficacy of various packaging techniques and thermal management strategies.

### 54.1.5 Chip Module Thermal Resistances

#### Definition

The thermal performance of alternative chip and packaging techniques is commonly compared on the basis of the overall (junction-to-coolant) thermal resistance, $R_T$. This packaging figure-of-merit is generally defined in a purely empirical fashion,

$$R_T \equiv \frac{T_j - T_{fl}}{q_c} \quad \text{(K/W)} \tag{54.24}$$

where $T_j$ and $T_{fl}$ are the junction and coolant (fluid) temperatures, respectively, and $q_c$ is the chip heat dissipation.

Unfortunately, however, most measurement techniques are incapable of detecting the actual junction temperature, that is, the temperature of the small volume at the interface of p-type and n-type semiconductors. Hence, this term generally refers to the average temperature or a representative temperature on the chip. To lower chip temperature at a specified power dissipation, it is clearly necessary to select and/or design a chip package with the lowest thermal resistance.

Examination of various packaging techniques reveals that the junction-to-coolant thermal resistance is, in fact, composed of an internal, largely conductive, resistance and an external, primarily convective, resistance. As shown in Fig. 54.3, the internal resistance, $R_{jc}$, is encountered in the flow of dissipated heat from the active chip surface through the materials used to support and bond the chip and on to the case of the integrated circuit package. The flow of heat from the case directly to the coolant, or indirectly through a fin structure and then to the coolant, must overcome the external resistance, $R_{ex}$.

The thermal design of single-chip packages, including the selection of die-bond, heat spreader, substrate, and encapsulant materials, as well as the quality of the bonding and encapsulating processes, can be characterized by the internal, or so-called junction–to–case, resistance. The convective heat removal techniques applied to the external surfaces of the package, including the effect of finned heat sinks and other thermal enhancements, can be compared on the basis of the external thermal resistance. The complexity of heat flow and coolant flow paths in a multichip module generally requires that the thermal capability of these packaging configurations be examined on the basis of overall, or chip-to-coolant, thermal resistance.

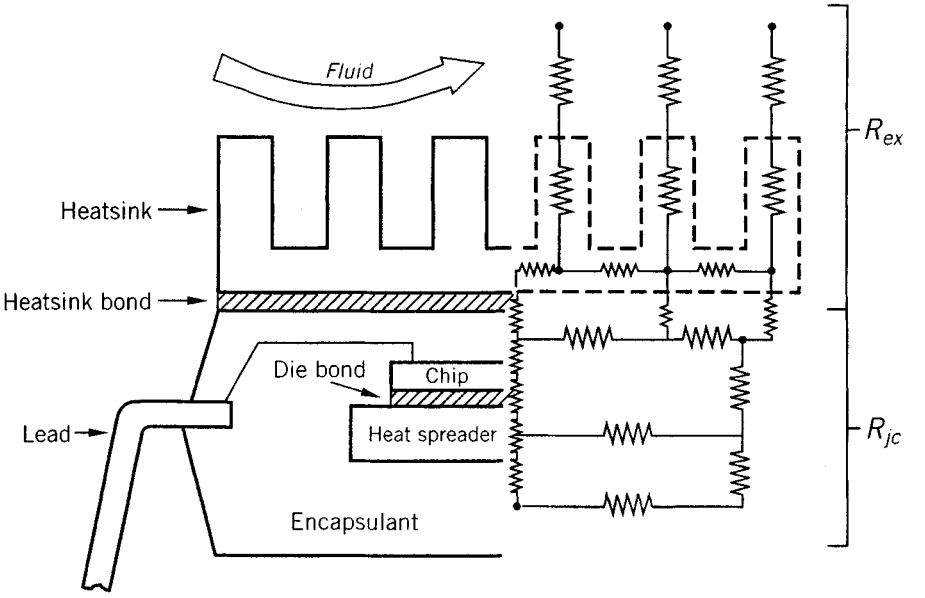


**Fig. 54.3** Primary thermal resistances in a single chip package.

### Internal Thermal Resistance

As discussed in Section 54.1.2, conductive thermal transport is governed by the Fourier equation, which can be used to define a conduction thermal resistance, as in Eq. (54.3). In flowing from the chip to the package surface or case, the heat encounters a series of resistances associated with individual layers of materials such as silicon, solder, copper, alumina, and epoxy, as well as the contact resistances that occur at the interfaces between pairs of materials. Although the actual heat flow paths within a chip package are rather complex and may shift to accommodate varying external cooling situations, it is possible to obtain a first-order estimate of the internal resistance by assuming that power is dissipated uniformly across the chip surface and that heat flow is largely one-dimensional. To the accuracy of these assumptions,

$$R_{jc} = \frac{T_j - T_c}{qc} = \sum \frac{x}{kA} \quad \text{(K/W)} \tag{54.25}$$

can be used to determine the internal chip module resistance where the summed terms represent the conduction thermal resistances posed by the individual layers, each with thickness $x$. As the thickness of each layer decreases and/or the thermal conductivity and cross-sectional area increase, the resistance of the individual layers decreases. Values of $R_{cd}$ for packaging materials with typical dimensions can be found via Eq. (54.25) or Fig 54.4, to range from 2 K/W for a 1000 mm$^2$ by 1 mm thick layer of epoxy encapsulant to 0.0006 K/W for a 100 mm$^2$ by 25 micron (1 mil) thick layer of copper. Similarly, the values of conduction resistance for typical "soft" bonding materials are found to lie in the range of approximately 0.1 K/W for solders and 1–3 K/W for epoxies and thermal pastes for typical $x/A$ ratios of 0.25 to 1.0.

Commercial fabrication practice in the late 1990s yields internal chip package thermal resistances varying from approximately 80 K/W for a plastic package with no heat spreader to 15–20 K/W for a plastic package with heat spreader, and to 5–10 K/W for a ceramic package or an especially designed plastic chip package. Large and/or carefully designed chip packages can attain even lower values of $R_{jc}$, down perhaps to 2 K/W.

Comparison of theoretical and experimental values of $R_{jc}$ reveals that the resistances associated with compliant, low-thermal-conductivity bonding materials and the spreading resistances, as well as

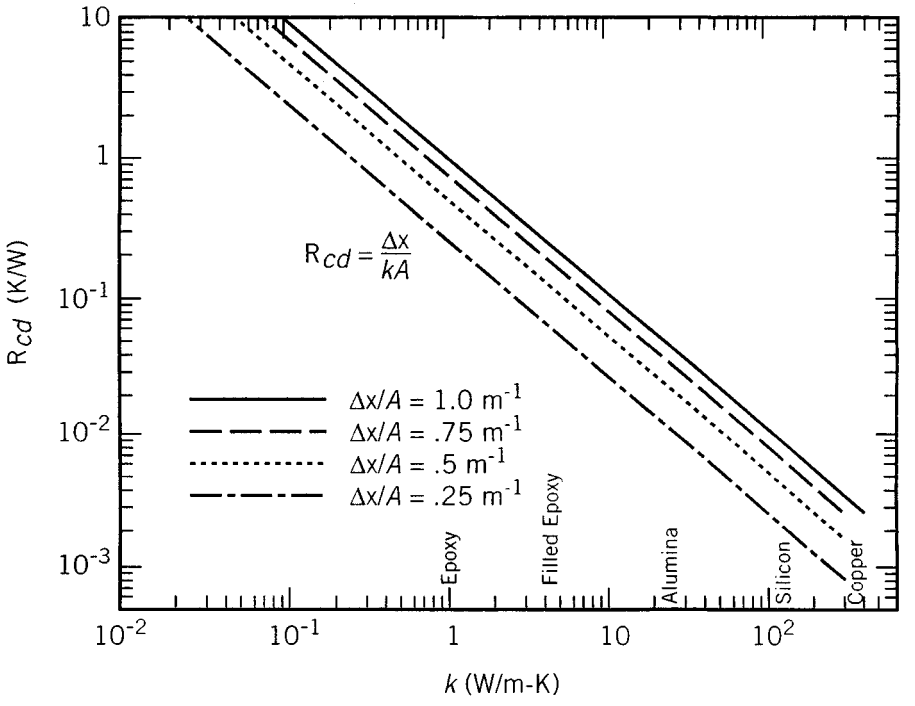


**Fig. 54.4** Conductive thermal resistance for packaging materials.

the contact resistances at the lightly loaded interfaces within the package, often dominate the internal thermal resistance of the chip package. It is thus not only necessary to determine the bond resistance correctly but also to add the values of $R_{sp}$, obtained from Eq. (54.6) and/or Fig. 54.1, and $R_{co}$ from Eq. (54.7b) or (54.9) to the junction–to–case resistance calculated from Eq. (54.25). Unfortunately, the absence of detailed information on the voidage in the die-bonding and heat-sink attach layers and the present inability to determine, with precision, the contact pressure at the relevant interfaces, conspire to limit the accuracy of this calculation.

### Substrate or PCB Conduction

In the design of airborne electronic systems and equipment to be operated in a corrosive or damaging environment, it is often necessary to conduct the heat dissipated by the components down into the substrate or printed circuit board and, as shown in Fig. 54.5, across the substrate/PCB to a cold plate or sealed heat exchanger. For a symmetrically cooled substrate/PCB with approximately uniform heat dissipation on the surface, a first estimate of the peak temperature, at the center of the board, can be obtained by use of Eq. (54.5).

Setting the heat generation rate equal to the heat dissipated by all the components and using the volume of the board in the denominator, the temperature difference between the center at $T_{ctr}$ and the edge of the substrate/PCB at $T_o$ is given by

$$T_{ctr} - T_o = \left(\frac{Q}{LW\delta}\right)\left(\frac{L^2}{8k_e}\right) = \frac{QL}{8W\delta k_e} \tag{54.26}$$

where $Q$ is the total heat dissipation, $W$, $L$, and $\delta$ are the width, length, and thickness, respectively, and $k_e$ is the effective thermal conductivity of the board.

This relation can be used effectively in the determination of the temperatures experienced by conductively cooled substrates and conventional printed circuit boards, as well as PCBs with copper lattices on the surface, metal cores, or heat sink plates in the center. In each case it is necessary to evaluate or obtain the effective thermal conductivity of the conducting layer. As an example, consider an alumina substrate 0.20 m long, 0.15 m wide and 0.005 m thick with a thermal conductivity of 20 W/m · K, whose edges are cooled to 35°C by a cold-plate. Assuming that the substrate is populated by 30 components, each dissipating 1 W, use of Eq. (54.26) reveals that the substrate center temperature will equal 85°C.

### External Resistance

To determine the resistance to thermal transport from the surface of a component to a fluid in motion, that is, the convective resistance as in Eq. (54.11), it is necessary to quantify the heat transfer coefficient, $h$. In the natural convection air cooling of printed circuit board arrays, isolated boards, and individual components, it has been found possible to use smooth-plate correlations, such as

$$h = C\left(\frac{k_{fl}}{L}\right)\mathrm{Ra}^n \tag{54.27}$$

and

$$h = \frac{k_{fl}}{b}\left[\frac{576}{(El')^2} + \frac{2.073}{(El')^{0.5}}\right]^{-1/2} \tag{54.28}$$

to obtain a first estimate of the peak temperature likely to be encountered on the populated board. Examination of such correlations suggests that an increase in the component/board temperature and a reduction in its length will serve to modestly increase the convective heat transfer coefficient and thus to modestly decrease the resistance associated with natural convection. To achieve a more dra-

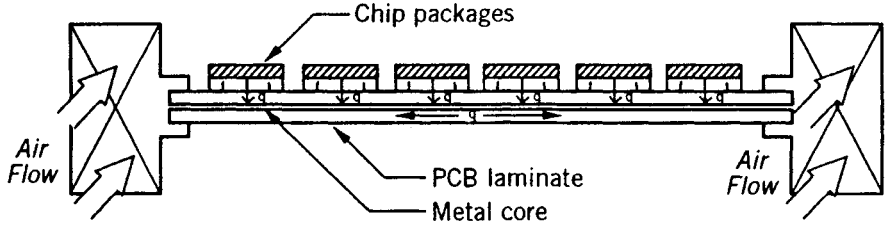


**Fig. 54.5** Edge-cooled printed circuit board populated with components.

matic reduction in this resistance, it is necessary to select a high density coolant with a large thermal expansion coefficient—typically a pressurized gas or a liquid.

When components are cooled by forced convection, the laminar heat transfer coefficient, given by Eq. (54.17), is found to be directly proportional, to the square root of fluid velocity and inversely proportional to the square root of the characteristic dimension. Increases in the thermal conductivity of the fluid and in Pr, as are encountered in replacing air with a liquid coolant, will also result in higher heat transfer coefficients. In studies of low-velocity convective air cooling of simulated integrated circuit packages, the heat transfer coefficient, $h$, has been found to depend somewhat more strongly on Re (using channel height as the characteristic length) than suggested in Eq. (54.17), and to display a Reynolds number exponent of 0.54 to 0.72.[8-10] When the fluid velocity and the Reynolds number increase, turbulent flow results in higher heat transfer coefficients, which, following Eq. (54.19), vary directly with the velocity to the 0.8 power and inversely with the characteristic dimension to the 0.2 power. The dependence on fluid conductivity and Pr remains unchanged.

An application of Eq. (54.27) or (54.28) to the transfer of heat from the case of a chip module to the coolant shows that the external resistance, $R_{ex} = 1/hS$, is inversely proportional to the wetted surface area and to the coolant velocity to the 0.5 to 0.8 power and directly proportional to the length scale in the flow direction to the 0.5 to 0.2 power. It may thus be observed that the external resistance can be strongly influenced by the fluid velocity and package dimensions and that these factors must be addressed in any meaningful evaluation of the external thermal resistances offered by various packaging technologies.

Values of the external resistance, for a variety of coolants and heat transfer mechanisms are shown in Fig. 54.6 for a typical component wetted area of 10 cm$^2$ and a velocity range of 2–8 m/s. They are seen to vary from a nominal 100 K/W for natural convection in air, to 33 K/W for forced convection in air, to 1 K/W in fluorocarbon liquid forced convection, and to less than 0.5 K/W for boiling in fluorocarbon liquids. Clearly, larger chip packages will experience proportionately lower external resistances than the displayed values. Moreover, conduction of heat through the leads and package base into the printed circuit board or substrate will serve to further reduce the effective thermal resistance.

In the event that the direct cooling of the package surface is inadequate to maintain the desired chip temperature, it is common to attach finned heat sinks, or compact heat exchangers, to the chip package. These heat sinks can considerably increase the wetted surface area, but may act to reduce the convective heat transfer coefficient by obstructing the flow channel. Similarly, the attachment of a heat sink to the package can be expected to introduce additional conductive resistances, in the

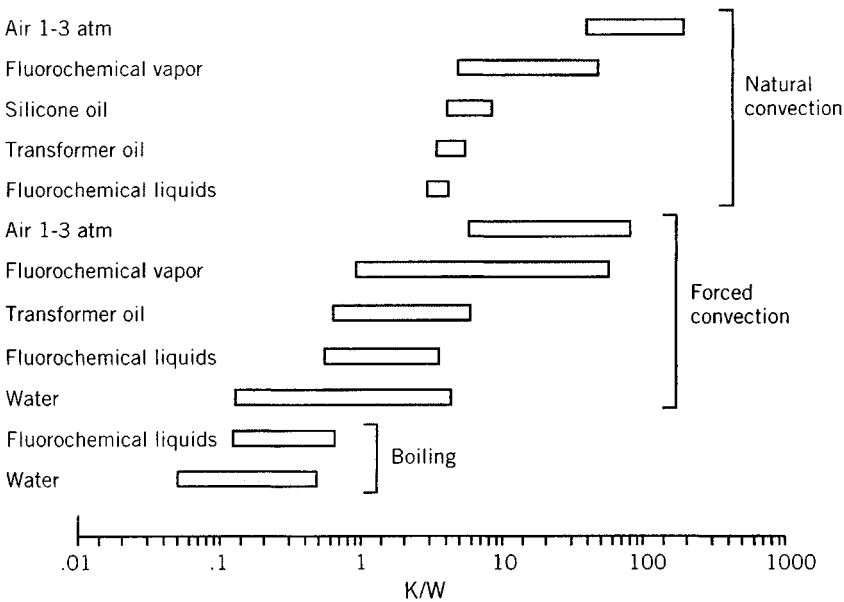


Note: For wetted area = 10 cm$^2$

**Fig. 54.6** Typical external (convective) thermal resistances for various coolants and cooling nodes.

adhesive used to bond the heat sink and in the body of the heat sink. Typical air-cooled heat sinks can reduce the external resistance to approximately 15 K/W in natural convection and to as low as 5 K/W for moderate forced convection velocities.

When a heat sink or compact heat exchanger is attached to the package, the external resistance accounting for the bond-layer conduction and the total resistance of the heat sink, $R_{sk}$, can be expressed as

$$R_{ex} = \frac{T_c - T_{fl}}{q_c} = \sum \left(\frac{x}{kA}\right)_b + R_{sk} \qquad \text{(K/W)} \tag{54.29}$$

where $R_{sk}$

$$R_{sk} = \left[\frac{1}{nhS_f\eta} + \frac{1}{h_bS_b}\right]^{-1}$$

is the the parallel combination of the resistance of the $n$ fins

$$R_f = \frac{1}{nhS_f\eta}$$

and the *bare* or base surface not occupied by the fins

$$R_b = \frac{1}{h_bS_b}$$

Here, the base surface is $S_b = S - S_f$ and the heat transfer coefficient, $h_b$, is used because the heat transfer coefficient that is applied to the base surfaces is not necessarily equal to that applied to the fins.

An alternative expression for $R_{sk}$ involves and *overall surface efficiency,* $\eta_o$, defined by

$$\eta_o = 1 - \frac{nS_f}{S}(1 - \eta)$$

where $S$ is the total surface composed of the base surface and the finned surfaces of $n$ fins

$$S = S_b + nS_f$$

In this case, it is presumed that $h_b = h$ so that

$$R_{sk} = \frac{1}{h\eta_oS}$$

In an optimally designed fin structure, $\eta$ can be expected to fall in the range of 0.50 to 0.70.[11] Relatively thick fins in a low-velocity flow of gas are likely to yield fin efficiencies approaching unity. This same unity value would be appropriate, as well, for an unfinned surface and, thus, serve to generalize the use of Eq. (54.29) to all package configurations.

### Flow Resistance

In convectively cooled systems, determination of the component temperature requires knowledge of the fluid temperature adjacent to the component. The rise in fluid temperature relative to the inlet value can be expressed in a flow thermal resistance, as done in Eq. (54.19). When the coolant flow path traverses many individual components, care must be taken to use $R_{fl}$ with the total heat absorbed by the coolant along its path, rather than the heat dissipated by an individual component. For system-level calculations, aimed at determining the average component temperature, it is common to base the flow resistance on the average rise in fluid temperature, that is, one-half the value indicated by Eq. (54.19).

### Total Resistance—Single Chip Packages

To the accuracy of the assumptions employed in the preceding development, the overall single-chip package resistance, relating the chip temperature to the inlet temperature of the coolant, can be found by summing the internal, external, and flow resistances to yield

$$R_T = R_{jc} + R_{ex} + R_{fl} = \sum \frac{x}{kA} + R_{int} + R_{sp} + R_{sk} + \left(\frac{Q}{q}\right)\left(\frac{1}{2\rho Q c_p}\right) \quad \text{(K/W)} \tag{54.30}$$

In evaluating the thermal resistance by this relationship, care must be taken to determine the effective cross-sectional area for heat flow at each layer in the module and to consider possible voidage in any solder and adhesive layers.

As previously noted in the development of the relationships for the external and internal resistances, Eq. (54.30) shows $R_T$ to be a strong function of the convective heat transfer coefficient, the flowing heat capacity of the coolant, and geometric parameters (thickness and cross-sectional area of each layer). Thus, the introduction of a superior coolant, use of thermal enhancement techniques that increase the local heat transfer coefficient, or selection of a heat transfer mode with inherently high heat transfer coefficients (boiling, for example) will all be reflected in appropriately lower external and total thermal resistances. Similarly, improvements in the thermal conductivity and reduction in the thickness of the relatively low-conductivity bonding materials (such as soft solder, epoxy or silicone) would act to reduce the internal and total thermal resistances.

Frequently, however, even more dramatic reductions in the total resistance can be achieved simply by increasing the cross-sectional area for heat flow within the chip module (such as chip, substrate and heat spreader) as well as along the wetted, exterior surface. The implementation of this approach to reducing the internal resistance generally results in a larger package footprint or volume but is rewarded with a lower thermal resistance. The use of heat sinks is, of course, the embodiment of this approach to the reduction of the external resistance.

## 54.2 HEAT-TRANSFER CORRELATIONS FOR ELECTRONIC EQUIPMENT COOLING

The reader should use the material in this section which pertains to heat-transfer correlations in geometries peculiar to electronic equipment in conjunction with the correlations provided in Chapter 43.

### 54.2.1 Natural Convection in Confined Spaces

For natural convection in confined horizontal spaces the recommended correlations for air are[12]

$$\begin{aligned} \text{Nu} &= 0.195(\text{Gr})^{1/4}, \quad 10^4 < \text{Gr} < 4 \times 10^5 \\ \text{Nu} &= 0.068(\text{Gr})^{1/3}, \quad \text{Gr} > 10^5 \end{aligned} \tag{54.31}$$

where Gr is the Grashof number,

$$\text{Gr} = \frac{g\rho^2\beta L^2 \Delta T}{\mu^2} \tag{54.32}$$

and where, in this case, the significant dimension $L$ is the gap spacing in both the Nusselt and Grashof numbers.

For liquids[13]

$$\text{Nu} = 0.069(\text{Gr})^{1/3}\text{Pr}^{0.407}, \quad 3 \times 10^5 < \text{Ra} < 7 \times 10^9 \tag{54.33a}$$

where Ra is the Rayleigh number,

$$\text{Ra} = \text{GrPr} \tag{54.33b}$$

For horizontal gaps with Gr < 1700, the conduction mode predominates and

$$h = \frac{k}{b} \tag{54.34}$$

where $b$ is the gap spacing. For 1700 < Gr < 10,000, use may be made of the Nusselt-Grashof relationship given in Fig. 54.7.[14,15]

For natural convection in confined vertical spaces containing air, the heat-transfer coefficient depends on whether the plates forming the space are operating under isoflux or isothermal conditions.[16]

For the symmetric isoflux case, a case that closely approximates the heat transfer in an array of printed circuit boards, the correlation for Nu is formed by using the method of Churchhill and Usagi[17] by considering the isolated plate case[18–20] and the fully developed limit:[21]

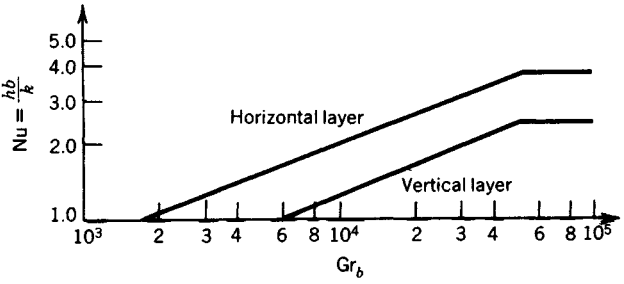


**Fig. 54.7** Heat transfer through enclosed air layers.[14,15]

$$\mathrm{Nu} = \left[\frac{12}{\mathrm{Ra}''} + \frac{1.88}{(\mathrm{Ra}'')^{2/5}}\right]^{-1/2} \tag{54.35}$$

where Ra″ is the modified channel Rayleigh number,

$$\mathrm{Ra}'' = \frac{g\beta p^2 q'' \mathrm{c}_p b^5}{\mu k^2 L} \tag{54.36}$$

The optimum spacing for the symmetrical isoflux case is

$$b_{\mathrm{opt}} = 1.472R^{-0.2} \tag{54.37}$$

where

$$R = \frac{g\beta p^2 c_p q''}{\mu k^2 L} \tag{54.38}$$

For the symmetric isothermal case, a case that closely approximates the heat transfer in a vertical array of extended surface or fins, the correlation is again formed using the Churchhill and Usagi[17] method by considering the isolated plate case[20] and the fully developed limit:[4,5,21]

$$\mathrm{Nu} = \left[\frac{576}{(\mathrm{Ra}')^2} + \frac{2.873}{(\mathrm{Ra}')^{1/2}}\right]^{-1/2} \tag{54.39}$$

where Ra′ is the channel Rayleigh number

$$\mathrm{Ra}' = \frac{g\beta p^2 c_p b^4}{\mu k L} \tag{54.40}$$

The optimum spacing for the symmetrical isothermal case is

$$b_{\mathrm{opt}} = \frac{2.714}{p^{1/4}} \tag{54.41}$$

where

$$P = \frac{g\beta p^2 c_p \Delta T}{\mu k L} \tag{54.42}$$

### 54.2.2 Forced Convection

#### External Flow on a Plane Surface

For an unheated starting length of the plane surface, $x_0$, in laminar flow, the local Nusselt number can be expressed by

**Table 54.1 Constants for Eq. 54.11**

| Reynolds Number Range | $B$ | $n$ |
|---|---|---|
| 1–4 | 0.891 | 0.330 |
| 4–40 | 0.821 | 0.385 |
| 40–4000 | 0.615 | 0.466 |
| 4000–40,000 | 0.174 | 0.618 |
| 40,000–400,000 | 0.0239 | 0.805 |

$$\mathrm{Nu}_x = \frac{0.332\mathrm{Re}^{1/2}\mathrm{Pr}^{1/3}}{[1 - (x_0/x)^{3/4}]^{1/3}} \tag{54.43}$$

Where Re is the Reynolds number, Pr is the Prandtl number, and Nu is the Nusselt number.

For flow in the inlet zones of parallel plate channels and along isolated plates, the heat transfer coefficient varies with L, the distance from the leading edge.[3] in the range $\mathrm{Re} \leq 3 \times 10^5$,

$$h = 0.664 \left(\frac{k_{fl}}{L}\right) \mathrm{Re}^{0.5}\mathrm{Pr}^{0.33} \tag{54.44}$$

and for $\mathrm{Re} > 3 \times 10^5$

$$h = 0.036 \left(\frac{k_{fl}}{L}\right) \mathrm{Re}^{0.8}\mathrm{Pr}^{0.33} \tag{54.45}$$

### Cylinders in Crossflow

For airflow around single cylinders at all but very low Reynolds numbers, Hilpert[23] has proposed

$$\mathrm{Nu} = \frac{hd}{k_f} = B\left(\frac{\rho V_\infty d}{\mu_f}\right)^n \tag{54.46}$$

where $V_\infty$ is the free stream velocity and where the constants $B$ and $n$ depend on the Reynolds number as indicated in Table 54.1.

It has been pointed out[12] that Eq. (54.46) assumes a natural turbulence level in the oncoming air stream and that the presence of augmentative devices can increase $n$ by as much as 50%. The modifications to $B$ and $n$ due to some of these devices are displayed in Table 54.2.

Equation (54.46) can be extended to other fluids[24] spanning a range of $1 < \mathrm{Re} < 10^5$ and $0.67 < \mathrm{Pr} < 300$:

$$\mathrm{Nu} = \frac{hd}{k} = (0.4\mathrm{Re}^{0.5} + 0.06\mathrm{Re}^{0.67})\mathrm{Pr}^{0.4}\left(\frac{\mu}{\mu_w}\right)^{0.25} \tag{54.47}$$

where all fluid properties are evaluated at the free stream temperature except $\mu_w$, which is the fluid viscosity at the wall temperature.

### Noncircular Cylinders in Crossflow

It has been found[12] that Eq. (54.46) may be used for noncircular geometries in crossflow provided that the characteristic dimension in the Nusselt and Reynolds numbers is the diameter of a cylinder having the same wetted surface equal to that of the geometry of interest and that the values of $B$ and $n$ are taken from Table 54.3.

**Table 54.2 Flow Disturbance Effects on $B$ and $n$ in Eq. (54.42)**

| Disturbance | Re Range | $B$ | $n$ |
|---|---|---|---|
| 1. Longitudinal fin, $0.1d$ thick on front of tube | 1000–4000 | 0.248 | 0.603 |
| 2. 12 longitudinal grooves, $0.7d$ wide | 3500–7000 | 0.082 | 0.747 |
| 3. Same as 2 with burrs | 3000–6000 | 0.368 | 0.86 |

**Table 54.3 Values of $B$ and $n$ for Eq. (54.46)[a]**

| Flow Geometry | $B$ | $n$ | Range of Reynolds Number |
|---|---|---|---|
| | 0.224 | 0.612 | 2,500–15,000 |
| | 0.085 | 0.804 | 3,000–15,000 |
| ◇ | 0.261 | 0.624 | 2,500–7,500 |
| ◇ | 0.222 | 0.588 | 5,000–100,000 |
| □ | 0.160 | 0.699 | 2,500–8,000 |
| □ | 0.092 | 0.675 | 5,000–100,000 |
| ○ | 0.138 | 0.638 | 5,000–100,000 |
| ○ | 0.144 | 0.638 | 5,000–19,500 |
| ○ | 0.035 | 0.782 | 19,500–100,000 |
| \| | 0.205 | 0.731 | 4,000–15,000 |

[a]From Ref. 12.

### Flow across Spheres

For airflow across a single sphere, it is recommended that the average Nusselt number when $17 < \mathrm{Re} < 7 \times 10^4$ be determined from[22]

$$\mathrm{Nu} = \frac{hd}{k_f} = 0.37 \left(\frac{\rho V_\infty d}{\mu_f}\right)^{0.6} \tag{54.48}$$

and for $1 < \mathrm{Re} < 25$[25],

$$\mathrm{Nu} = \frac{hd}{k} = 2.2\mathrm{Pr} + 0.48\mathrm{Pr}(\mathrm{Re})^{0.5} \tag{54.49}$$

For both gases and liquids in the range $3.5 < \mathrm{Re} < 7.6 \times 10^4$ and $0.7 < \mathrm{Pr} < 380$[24]

$$\mathrm{Nu} = \frac{hd}{k} = 2 + (4.0\mathrm{Re}^{0.5} + 0.06\mathrm{Re}^{0.67})\mathrm{Pr}^{0.4} \left(\frac{\mu}{\mu_w}\right)^{0.25} \tag{54.50}$$

### Flow across Tube Banks

For the flow of fluids flowing normal to banks of tubes,[26]

$$\mathrm{Nu} = \frac{hd}{k_f} = C \left(\frac{\rho V_\infty d}{\mu_f}\right)^{0.6} \left(\frac{c_p \mu}{k}\right)_f^{0.33} \phi \tag{54.51}$$

which is valid in the range $2000 < \mathrm{Re} < 32{,}000$.

For in-line tubes, $C = 0.26$, whereas for staggered tubes, $C = 0.33$. The factor $\phi$ is a correction factor for sparse tube banks, and values of $\phi$ are provided in Table 54.4.

For air in the range where Pr is nearly constant ($\mathrm{Pr} \simeq 0.7$ over the range 25–200°C), Eq. (54.51) can be reduced to

$$\mathrm{Nu} = \frac{hd}{k_f} = C' \left(\frac{\rho V_\infty d}{\mu_f}\right)^{n'} \tag{54.52}$$

where $C'$ and $n'$ may be determined from values listed in Table 54.5. This equation is valid in the range $2000 < \mathrm{Re} < 40{,}000$ and the ratios $x_L$ and $x_T$ denote the ratio of centerline diameter to tube spacing in the longitudinal and transverse directions, respectively.

For fluids other than air, the curve shown in Fig. 54.8 should be used for staggered tubes.[22] For in-line tubes, the values of

$$j = \left(\frac{hd_0}{k}\right) \left(\frac{c_p \mu}{k}\right)^{-1/3} \left(\frac{\mu}{\mu_w}\right)^{-0.14}$$

should be reduced by 10%.

**Table 54.4 Correlation Factor $\phi$ for Sparse Tube Banks**

| Number of Rows, $N$ | In Line | Staggered |
|---|---|---|
| 1 | 0.64 | 0.68 |
| 2 | 0.80 | 0.75 |
| 3 | 0.87 | 0.83 |
| 4 | 0.90 | 0.89 |
| 5 | 0.92 | 0.92 |
| 6 | 0.94 | 0.95 |
| 7 | 0.96 | 0.97 |
| 8 | 0.98 | 0.98 |
| 9 | 0.99 | 0.99 |
| 10 | 1.00 | 1.00 |

### Flow across Arrays of Pin Fins

For air flowing normal to banks of staggered cylindrical pin fins or spines,[28]

$$\text{Nu} = \frac{hd}{k} = 1.40 \left(\frac{\rho v_\infty d}{\mu}\right)^{0.8} \left(\frac{c_p \mu}{k}\right)^{1/3} \tag{54.53}$$

### Flow of Air over Electronic Components

For single prismatic electronic components, either normal or parallel to the sides of the component in a duct,[29] for $2.5 \times 10^3 < \text{Re} < 8 \times 10^3$,

$$\text{Nu} = 0.446 \left[\frac{\text{Re}}{(1/6) + (5A_n/6A_0)}\right]^{0.57} \tag{54.54}$$

where the Nusselt and Reynolds numbers are based on the prism side dimension and where $A_0$ and $A_n$ are the gross and net flow areas, respectively.

For staggered prismatic components, Eq. (54.54) may be modified to[29]

$$\text{Nu} = 0.446 \left[\frac{\text{Re}}{(1/6) + (5A_n/A_0)}\right]^{0.57} \left[1 + 0.639 \left(\frac{S_T}{S_{T,\max}}\right) \left(\frac{d}{S_L}\right)^{0.172}\right] \tag{54.55}$$

**Table 54.5 Values of the Constants $C'$ and $n'$ in Eq. (54.52)**

| $x_L = \frac{S_L}{d_0}$ | $x_T = \frac{S_T}{d_0} = 1.25$ | | $x_T = \frac{S_T}{d_0} = 1.50$ | | $x_T = \frac{S_T}{d_0} = 2.00$ | | $x_T = \frac{S_T}{d_0} = 3.00$ | |
|---|---|---|---|---|---|---|---|---|
| | $C'$ | $n'$ | $C'$ | $n'$ | $C'$ | $n'$ | $C'$ | $n'$ |
| *Staggered* | | | | | | | | |
| 0.600 | | | | | | | 0.213 | 0.636 |
| 0.900 | | | | | 0.446 | 0.571 | 0.401 | 0.581 |
| 1.000 | | | 0.497 | 0.558 | | | | |
| 1.125 | | | | | 0.478 | 0.565 | 0.518 | 0.560 |
| 1.250 | 0.518 | 0.556 | 0.505 | 0.554 | 0.519 | 0.556 | 0.522 | 0.562 |
| 1.500 | 0.451 | 0.568 | 0.460 | 0.562 | 0.452 | 0.568 | 0.488 | 0.568 |
| 2.000 | 0.404 | 0.572 | 0.416 | 0.568 | 0.482 | 0.556 | 0.449 | 0.570 |
| 3.000 | 0.310 | 0.592 | 0.356 | 0.580 | 0.440 | 0.562 | 0.421 | 0.574 |
| *In Line* | | | | | | | | |
| 1.250 | 0.348 | 0.592 | 0.275 | 0.608 | 0.100 | 0.704 | 0.0633 | 0.752 |
| 1.500 | 0.367 | 0.586 | 0.250 | 0.620 | 0.101 | 0.702 | 0.0678 | 0.744 |
| 2.000 | 0.418 | 0.570 | 0.299 | 0.602 | 0.229 | 0.632 | 0.198 | 0.648 |
| 3.000 | 0.290 | 0.601 | 0.357 | 0.584 | 0.374 | 0.581 | 0.286 | 0.608 |

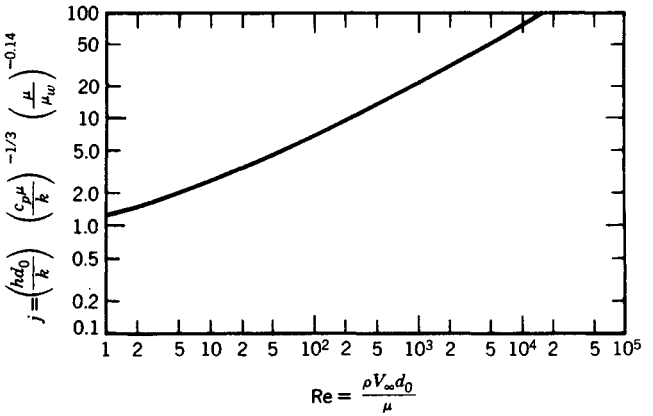


**Fig. 54.8** Recommended curve for estimation of heat transfer coefficient for fluids flowing normal to staggered tubes 10 rows deep (from Ref. 22).

where $d$ is the prism side dimension, $S_L$ is the longitudinal separation, $S_T$ is the transverse separation, and $S_{T,\max}$ is the maximum transverse spacing if different spacings exist.

When cylindrical heat sources are encountered in electronic equipment, a modification of Eq. (54.46) has been proposed:[30]

$$\mathrm{Nu} = \frac{hd}{k_f} = FB\left(\frac{\rho V_\infty d}{\mu}\right)^n \tag{54.56}$$

where $F$ is an arrangement factor depending on the cylinder geometry (see Table 54.6) and where the constants $B$ and $n$ are given in Table 54.7.

### Forced Convection in Tubes, Pipes, Ducts, and Annuli

For heat transfer in tubes, pipes, ducts, and annuli, use is made of the equivalent diameter

$$d_e = \frac{4A}{WP} \tag{54.57}$$

in the Reynolds and Nusselt numbers unless the cross section is circular, in which case $d_e$ and $d_i = d$.

In the laminar regime[31] where $\mathrm{Re} < 2100$,

**Table 54.6 Values of $F$ to Be Used in Eq. (54.56)[a]**

Single cylinder in free stream: $F = 1.0$
Single cylinder in duct: $F = 1 + d/w$
In-line cylinders in duct:

$$F = \left(1 + \sqrt{\frac{1}{S_T}}\right)\left\{1 + \left(\frac{1}{S_L} - \frac{0.872}{S_L^2}\right)\left(\frac{1.81}{S_T^2} - \frac{1.46}{S_T} + 0.318\right)\left[\mathrm{Re}^{0.526-(0.354/S_T)}\right]\right\}$$

Staggered cylinders in duct:

$$F = \left(1 + \sqrt{\frac{1}{S_T}}\right)\left\{1 + \left[\frac{1}{S_L}\left(\frac{15.50}{S_T^2} - \frac{16.80}{S_T} + 4.15\right) - \frac{1}{S_L}\left(\frac{14.15}{S_T^2} - \frac{15.33}{S_T} + 3.69\right)\right]\mathrm{Re}^{0.13}\right\}$$

[a]Re to be evaluated at film temperature. $S_L$ = ratio of longitudinal spacing to cylinder diameter. $S_T$ = ratio of transverse spacing to cylinder diameter.

**Table 54.7 Values of $B$ and $n$ for Use in Eq. (54.56)**

| Reynolds Number Range | $B$ | $n$ |
|---|---|---|
| 1000–6000 | 0.409 | 0.531 |
| 6000–30,000 | 0.212 | 0.606 |
| 30,000–100,000 | 0.139 | 0.806 |

$$\text{Nu} = hd_e/k = 1.86[\text{RePr}(d_e/L)]^{1/3}(\mu/\mu_w)^{0.14} \tag{54.58}$$

with all fluid properties except $\mu_w$ evaluated at the bulk temperature of the fluid.

For Reynolds numbers above transition, Re > 2100,

$$\text{Nu} = 0.023(\text{Re})^{0.8}(\text{Pr})^{1/3}(\mu/\mu_w)^{0.14} \tag{54.59}$$

and in the transition region, 2100 < Re < 10,000,[32]

$$\text{Nu} = 0.116[(\text{Re})^{2/3} - 125](\text{Pr})^{1/3}(\mu/\mu_w)^{0.14}[1 + (d_e/L)^{2/3}] \tag{54.60}$$

London[33] has proposed a correlation for the flow of air in rectangular ducts. It is shown in Fig. 54.9. This correlation may be used for air flowing between longitudinal fins.

## 54.3 THERMAL CONTROL TECHNIQUES

### 54.3.1 Extended Surface and Heat Sinks

The heat flux from a surface, $q/A$, can be reduced if the surface area $A$ is increased. The use of extended surface or fins in a common method of achieving this reduction. Another way of looking at this is through the use of Newton's law of cooling:

$$q = hA\Delta T \tag{54.61}$$

and considering that $\Delta T$ can be reduced for a given heat flow $q$ by increasing $h$, which is difficult for a specified coolant, or by increasing the surface area $A$.

The common extended surface shapes are the longitudinal fin of rectangular profile, the radial fin of rectangular profile, and the cylindrical spine shown, respectively, in Figs. 54.10*a*, *e*, and *g*.

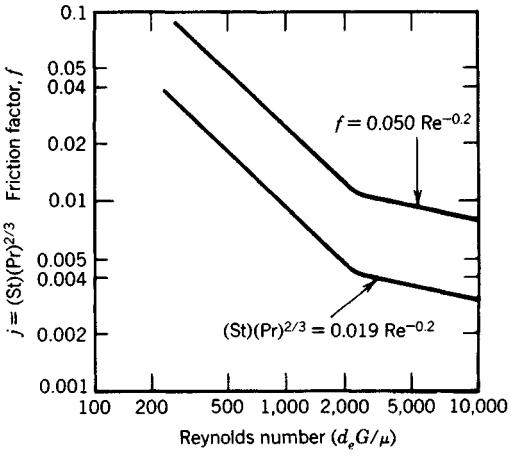


**Fig. 54.9** Heat transfer and friction data for forced air through rectangular ducts. St is the stanton number, $\text{St} = hG/c_p$.

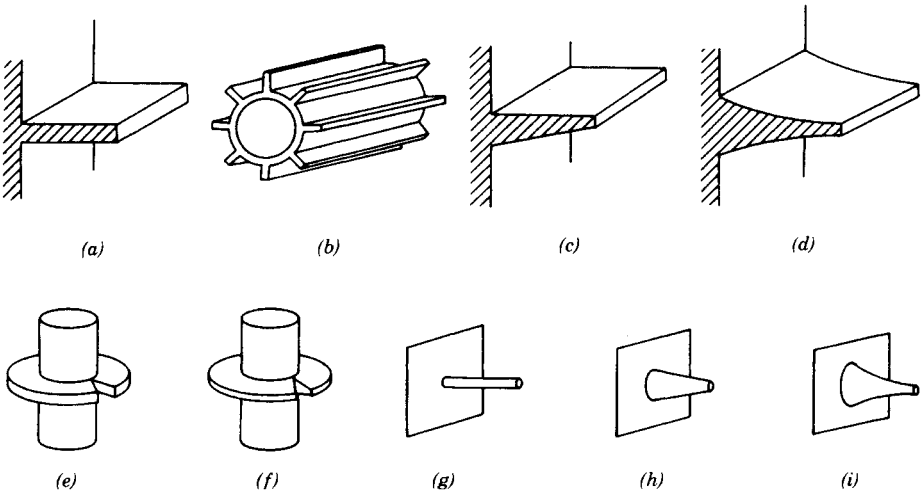


**Fig. 54.10** Some typical examples of extended surfaces: (*a*) longitudinal fin of rectangular profile: (*b*) cylindrical tube equipped with longitudinal fins; (c) longitudinal fin of trapezoidal profile; (*d*) longitudinal fin of truncated concave parabolic profile; (*e*) cylindrical tube equipped with radial fin of rectangular profile; (*f*) cylindrical tube equipped with radial fin of truncated triangular profile; (*g*) cylindrical spine; (*h*) truncated conical spine; (*i*) truncated concave parabolic spine.

### Assumptions in Extended Surface Analysis

The analysis of extended surface is subject to the following simplifying assumptions:[34,35]

1. The heat flow is steady; that is, the temperature at any point does not vary with time.
2. The fin material is homogeneous, and the thermal conductivity is constant and uniform.
3. The coefficient of heat transfer is constant and uniform over the entire face surface of the fin.
4. The temperature of the surrounding fluid is constant and uniform.
5. There are no temperature gradients within fin other than along the fin height.
6. There is no bond resistance to the flow of heat at the base of the fin.
7. The temperature at the base of the fin is uniform and constant.
8. There are no heat sources within the fin itself.
9. There is a negligible flow of heat from the tip and sides of the fin.
10. The heat flow from the fin is proportioned to the temperature difference or temperature excess, $\theta(x) = T(x) - T_s$, at any point on the face of the fin.

### The Fin Efficiency

Because a temperature gradient always exists along the height of a fin when heat is being transferred to the surrounding environment by the fin, there is a question regarding the temperature to be used in Eq. (54.61). If the base temperature $T_b$ (and the base temperature excess, $\theta_b = T_b - T_s$) is to be used, then the surface area of the fin must be modified by the computational artifice known as the fin efficiency, defined as the ratio of the heat actually transferred by the fin to the ideal heat transferred if the fin were operating over its entirety at the base temperature excess. In this case, the surface area $A$ in Eq. (54.43) becomes

$$A = A_b + \eta_f A_f \tag{54.62}$$

### The Longitudinal Fin of Rectangular Profile

With the origin of the height coordinate $x$ taken at the fin tip, which is presumed to be adiabatic, the temperature excess at any point on the fin is

$$\theta(x) = \theta_b \frac{\cosh mx}{\cosh mb} \tag{54.63}$$

where

$$m = \left(\frac{2h}{k\delta}\right)^{1/2} \tag{54.64}$$

The heat dissipated by the fin is

$$q_b = Y_0 \theta_b \tanh mb \tag{54.65}$$

where $Y_0$ is called the characteristic admittance

$$Y_0 = (2hk\delta)^{1/2} L \tag{54.66}$$

and the fin efficiency is

$$\eta_f = \frac{\tanh mb}{mb} \tag{54.67}$$

The heat-transfer coefficient in natural convection may be determined from the symmetric isothermal case pertaining to vertical plates in Section 54.2.1. For forced convection, the London correlation described in Section 54.2.2 applies.

### The Radial Fin of Rectangular Profile

With the origin of the radial height coordinate taken at the center of curvature and with the fin tip at $r = r_a$ presumed to be adiabatic, the temperature excess at any point on the fin is

$$\theta(r) = \theta_b \left[\frac{K_1(mr_a)I_0(mr) + I_1(mr_a)K_0(mr)}{I_0(mr_b)K_1(mr_a) + I_1(mr_a)K_0(mr_b)}\right] \tag{54.68}$$

where $m$ is given by Eq. (54.64). The heat dissipated by the fin is

$$q_b = 2\pi r_b km\theta_b \left[\frac{I_1(mr_a)K_1(mr_b) - K_1(mr_a)I_1(mr_b)}{I_0(mr_b)K_1(mr_a) + I_1(mr_a)K_0(mr_b)}\right] \tag{54.69}$$

and the fin efficiency is

$$\eta f = \frac{2r_b}{m(r_a^2 - r_b^2)} \left[\frac{I_1(mr_a)K_1(mr_b) - K_1(mr_a)I_1(mr_b)}{I_0(mr_b)K_1(mr_a) + I_1(mr_a)K_0(mr_b)}\right] \tag{54.70}$$

Tables of the fin efficiency are available,[36] and they are organized in terms of two parameters, the radius ratio

$$\rho = \frac{r_b}{r_a} \tag{54.71a}$$

and a parameter $\phi$

$$\phi = (r_a - r_b)\left(\frac{2h}{kA_p}\right)^{1/2} \tag{54.71b}$$

where $A_p$ is the profile area of the fin:

$$A_p = \delta(r_a - r_b) \tag{54.71c}$$

For air under forced convection conditions, the correlation for the heat-transfer coefficient developed by Briggs and Young[37] is applicable:

$$\frac{h}{2r_b k} = \left(\frac{2\rho V r_b}{\mu}\right)^{0.681} \left(\frac{c_p \mu}{k}\right)^{1/3} \left(\frac{s}{r_a - r_b}\right)^{0.200} \left(\frac{s}{\delta}\right)^{0.1134} \tag{54.72}$$

where all thermal properties are evaluated at the bulk air temperature, $s$ is the space between the fins, and $r_a$ and $r_b$ pertain to the fins.

### The Cylindrical Spine

With the origin of the height coordinate $x$ taken at the spine tip, which is presumed to be adiabatic, the temperature excess at any point on the spine is given by Eq. (54.61), but for the cylindrical spine

$$m = \left(\frac{4h}{kd}\right)^{1/2} \tag{54.73}$$

where $d$ is the spine diameter. The heat dissipated by the spine is given by Eq. (54.65), but in this case

$$Y_0 = (\pi^2 hkd^3)^{1/2}/2 \tag{54.74}$$

and the spine efficiency is given by Eq. (54.67).

### Algorithms for Combining Single Fins into Arrays

The differential equation for temperature excess that can be developed for any fin shape can be solved to yield a particular solution, based on prescribed initial conditions of fin base temperature excess and fin base heat flow, that can be written in matrix form[38,39] as

$$\begin{bmatrix} \theta_a \\ q_a \end{bmatrix} = [\Gamma] \begin{bmatrix} \theta_b \\ q_b \end{bmatrix} = \begin{bmatrix} \gamma_{11} & \gamma_{12} \\ \gamma_{21} & \gamma_{22} \end{bmatrix} \begin{bmatrix} \theta_b \\ q_b \end{bmatrix} \tag{54.75}$$

The matrix $[\Gamma]$ is called the thermal transmission matrix and provides a linear transformation from tip to base conditions. It has been cataloged for all of the common fin shapes.[38–40] For the longitudinal fin of rectangular profile

$$[\Gamma] = \begin{bmatrix} \cosh mb & -\dfrac{1}{Y_0} \sinh mb \\ -Y_0 \sinh mb & \cosh mb \end{bmatrix} \tag{54.76}$$

and this matrix possesses an inverse called the inverse thermal transmission matrix

$$[\Lambda] = [\Gamma]^{-1} = \begin{bmatrix} \cosh mb & \dfrac{1}{Y_0} \sinh mb \\ Y_0 \sinh mb & \cosh mb \end{bmatrix} \tag{54.77}$$

The assembly of fins into an array may require the use of any or all of three algorithms.[40–42] The objective is to determine the input admittance of the entire array

$$Y_{\text{in}} = \left.\frac{q_b}{\theta_b}\right|_A \tag{54.78}$$

which can be related to the array (fin) efficiency by

$$\eta_f = \frac{Y_{\text{in}}}{hA_f} \tag{54.79}$$

The determination of $Y_{\text{in}}$ can involve as many as three algorithms for the combination of individual fins into an array.

The Cascade Algorithm: For $n$ fins in cascade as shown in Fig. 54.11*a*, an equivalent inverse thermal transmission matrix can be obtained by a simple matrix multiplication, with the individual fins closest to the base of the array acting as permultipliers:

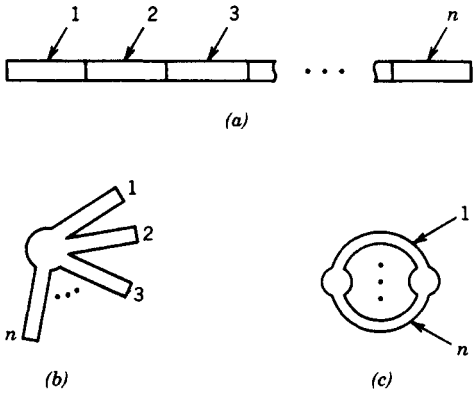


**Fig. 54.11** (*a*) $n$ fins in cascade, (*b*) $n$ fins in cluster, and (*c*) $n$ fins in parallel.

$$\{\Lambda\}_e = \{\Lambda\}_n\{\Lambda\}_{n-1}\{\Lambda\}_{n-2}\cdots\{\Lambda\}_2\{\Lambda\}_1 \tag{54.80}$$

For the case of the tip of the most remote fin adiabatic, the array input admittance will be

$$Y_{\text{in}} = \frac{\lambda_{21,e}}{\lambda_{11,e}} \tag{54.81}$$

If the tip of the most remote fin is not adiabatic, the heat flow to temperature excess ratio at the tip which is designated as $\mu$

$$\mu = \frac{q_a}{\theta_a} \tag{54.82}$$

will be known. For example, for a fin dissipating to the environment through its tip designated by the subscript $a$:

$$\mu = hA_a \tag{54.83}$$

In this case, $Y_{\text{in}}$ may be obtained through successive use of what is termed the reflection relationship (actually a bilinear transformation):

$$Y_{\text{in},k-1} = \frac{\lambda_{21,k-1} + \lambda_{22,k-1}(q_a/\theta_a)}{\lambda_{11,k-1} + \lambda_{12,k-1}(q_a/\theta_a)} \tag{54.84}$$

***The Cluster Algorithm.*** For $n$ fins in cluster, as shown in Fig. 54.11*b*, the equivalent thermal transmission ratio will be the sum of the individual fin input admittances:

$$\mu_e = \sum_{k=1}^{n} Y_{\text{in},k} = \sum_{k=1}^{n} \frac{q_b}{\theta_b}\bigg|_k \tag{54.85}$$

Here, $Y_{\text{in},k}$ can be determined for each individual fin via Eq. (54.82) if the fin has an adiabatic tip or via Eq. (54.84) if the tip is not adiabatic. It is obvious that this holds if subarrays containing more than one fin are in cluster.

***The Parallel Algorithm.*** For $n$ fins in parallel, as shown in Fig. 54.11*c*, an equivalent thermal admittance matrix $[Y]_e$ can be obtained from the sum of the individual thermal admittance matrices:

$$[Y]_e = \sum_{k=1}^{n} [Y]_k \tag{54.86}$$

where the individual thermal admittance matrices can be obtained from

$$[Y] = \begin{bmatrix} y_{11} & y_{12} \\ y_{21} & y_{22} \end{bmatrix} = \begin{bmatrix} -\dfrac{\gamma_{11}}{\gamma_{12}} & \dfrac{1}{\gamma_{12}} \\ -\dfrac{1}{\gamma_{12}} & \dfrac{\gamma_{22}}{\gamma_{12}} \end{bmatrix} = \begin{bmatrix} \dfrac{\lambda_{22}}{\lambda_{12}} & -\dfrac{1}{\lambda_{12}} \\ \dfrac{1}{\lambda_{12}} & -\dfrac{\lambda_{21}}{\lambda_{22}} \end{bmatrix} \tag{54.87}$$

If necessary, $[\Lambda]$ may be obtained from $[Y]$ using

$$[\Lambda] = \begin{bmatrix} \lambda_{11} & \lambda_{12} \\ \lambda_{21} & \lambda_{22} \end{bmatrix} = \begin{bmatrix} -\dfrac{y_{22}}{y_{21}} & \dfrac{1}{y_{21}} \\ -\dfrac{\Delta y}{y_{21}} & \dfrac{y_{11}}{y_{21}} \end{bmatrix} \tag{54.88}$$

where $\Delta_Y = y_{11}y_{22} - y_{12}y_{21}$

***Singular Fans.*** There will be occasions when a singular fin, one whose tip comes to a point, will be used as the most remote fin in an array. In this case the $[\Gamma]$ and $[\Lambda]$ matrices do not exist and the fin is characterized by its input admittance.[38–40] Such a fin is the longitudinal fin of triangular profile where

$$Y_{\text{in}} = \frac{q_b}{\theta_b} = \frac{2hI_1(2mb)}{mI_0(2mb)} \tag{54.89}$$

where

$$m = \left(\frac{2h}{k\delta_b}\right)^{1/2} \tag{54.90}$$

### 54.3.2 The Cold Plate

The cold plate heat exchanger or forced cooled electronic chassis is used to provide a "cold wall" to which individual components and, for that matter, entire packages of equipment may be mounted. Its design and performance evaluation follows a certain detailed procedure that depends on the type of heat loading and whether the heat loading is on one or two sides of the cold plate. These configurations are displayed in Fig. 54.12.

The design procedure is based on matching the available heat-transfer effectiveness $\epsilon$ to the required effectiveness $\epsilon$ determined from the design specifications. These effectivenesses are for the isothermal case in Fig. 54.12*a*

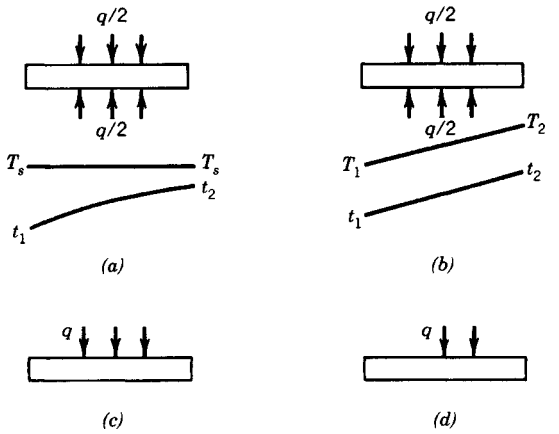


**Fig. 54.12** (*a*) Double-sided, evenly loaded cold plate—isothermal case; (*b*) double-sided, evenly loaded cold plate—isoflux case; (*c*) single-sided, evenly loaded cold plate—isothermal case; and (*d*) single-sided, evenly loaded cold plate—isoflux case.

$$\epsilon = \frac{t_2 - t_1}{T_s - t_1} = e^{-NTU} \tag{54.91}$$

and for the isoflux case in Fig. 69.12*b*

$$\epsilon = \frac{t_2 - t_1}{T_2 - t_1} \tag{54.92}$$

where the "number of transfer units" is

$$NTU = \frac{h\eta_0 A}{Wc_p} \tag{54.93}$$

and the overall passage efficiency is

$$\eta_0 = 1 - \frac{A_f}{A}(1 - \eta_f) \tag{54.94}$$

The surfaces to be used in the cold plate are those described by Kays and London[41] where physical, heat-transfer, and friction data are provided.

The detailed design procedure for the double-side-loaded isothermal case is as follows:

1. Design specification
   (a) Heat load, $q$, W
   (b) Inlet air temperature, $t_1$, °C
   (c) Airflow, $W$, kg/sec
   (d) Allowable pressure loss, cm $H_2O$
   (e) Overall envelope, $H$, $W$, $D$
   (f) Cold plate material thermal conductivity, $k_m$, W/m · °C
   (g) Allowable surface temperature, $T_s$, °C
2. Select surface[41]
   (a) Type
   (b) Plate spacing, $b$, m
   (c) Fins per meter, fpm
   (d) Hydraulic diameter, $d_e$, m
   (e) Fin thickness, $\delta$, m
   (f) Heat transfer area/volume, $\beta$, $m^2/m^3$
   (g) Fin surface area/total surface area, $A_f/A$, $m^2/m^3$
3. Plot of $j$ and $f$ data[41]

$$j = (\mathrm{St})(\mathrm{Pr})^{2/3} = f_1(\mathrm{Re}) = f_1\left(\frac{d_e G}{\mu}\right)$$

   where St is the Stanton number

$$\mathrm{St} = \frac{hG}{c_p} \tag{54.95}$$

   and $f$ is the friction factor

$$f = f_2(\mathrm{Re}) = f_2\left(\frac{d_e G}{\mu}\right)$$

4. Establish physical data
   (a) $a = (b/H)\beta$, $m^2/m^3$
   (b) $r_h = d_e/4$, m
   (c) $\sigma = ar_h$
   (d) $A_{fr} = WH$, $m^2$ (frontal area)
   (e) $A_c = \sigma A_{fr}$, $m^2$ (flow areas)
   (f) $V = DWH$ (volume)
   (g) $A = aV$, $m^2$ (total surface)

5. Heat balance
   (a) Assume average fluid specific heat, $c_p$, J/kg · °C
   (b) $\Delta t = t_2 - t_1 = q/Wc_p$, °C
   (c) $t_2 = t_1 + \Delta t$, °C
   (d) $t_{av} = \frac{1}{2}(t_1 + t_2)$
   (e) Check assumed value of $c_p$. Make another assumption if necessary
6. Fluid properties at $t_{av}$
   (a) $c_p$ (already known), J/kg · °C
   (b) $\mu$, N/sec · m$^2$
   (c) $k$, W/m · °C
   (d) $(\mathrm{Pr})^{2/3} = (c_p\mu/k)^{2/3}$
7. Heat-transfer coefficient
   (a) $G = W/A_c$, kg/sec · m$^2$
   (b) $\mathrm{Re} = d_e G/\mu$
   (c) Obtain $j$ from curve (see item 3)
   (d) Obtain $f$ from curve (see item 3)
   (e) $h = jGc_p/(\mathrm{Pr})^{2/3}$, W/m$^2$ · °C
8. Fin efficiency
   (a) $m = (2h/k\delta)^{1/2}$, m$^{-1}$
   (b) $mb/2$ is a computation
   (c) $\eta_f = (\tanh mb/2)/mb/2$
9. Overall passage efficiency
   (a) Use Eq. (54.94)
10. Effectiveness
    (a) Required $\epsilon = (t_2 - t_1)/(T_s - T_1)$
    (b) Form $NTU$ from Eq. (54.93)
    (c) Actual available $\epsilon = 1 - e^{-NTU}$
    (d) Compare required $\epsilon$ and actual $\epsilon$ and begin again with step 1 if the comparison fails. If comparison is satisfactory go on to pressure loss calculation.
11. Pressure loss
    (a) Establish $v_1$ (specific volume), m$^3$/k
    (b) Establish $v_2$, m$^3$/kg
    (c) $v_m = \frac{1}{2}(v_1 + v_2)$, m$^3$/kg
    (d) Form $v_m/v_1$
    (e) Form $v_2/v_1$
    (f) Obtain $K_c$ and $K_e$[41]
    (g) Determine $\Delta P$, cm

$$\Delta P = 0.489 \frac{G^2 v_1}{2g}\left[(1 + K_c - \sigma^2) + f\frac{A}{A_c}\frac{v_m}{v_1} + 2\left(\frac{v_2}{v_1} - 1\right) - (1 - \sigma^2 - K_c)\frac{v_2}{v_1}\right] \quad (54.96)$$

    (h) Compare $\Delta P$ with specified $\Delta P$. If comparison fails select a different surface or adjust the dimensions and begin again with step 1

If the cold plate is loaded on one side only, an identical procedure is followed except in steps 8 and 9. For single-side loading and for double and triple stacks, use must be made of the cascade and cluster algorithms for the combination of fins described in Section 54.3.1. Detailed examples of both of the foregoing cases may be found in Kraus and Bar-Cohen.[11]

### 54.3.3 Thermoelectric Coolers

Two thermoelectric effects are traditionally considered in the design and performance evaluation of a thermoelectric cooler:

The Seebeck effect concerns the net conversion of thermal energy into electrical energy under zero current conditions when two dissimilar materials are brought into contact. When the junction temperature differs from a reference temperature, the effect is measured as a voltage called the Seebeck voltage $E_s$.

The Peltier effect concerns the reversible evolution or absorption of heat that occurs when an electric current traverses the junction between two dissimilar materials. The Peltier heat absorbed or rejected depends on and is proportional to the current flow. There is an additional thermoelectric effect known as the Thomson effect, which concerns the reversible evolution or absorption of heat that occurs when an electric current traverses a single homogeneous material in the presence of a temperature gradient. This effect, however, is a negligible one and is neglected in considerations of thermoelectric coolers operating over moderate temperature differentials.

### Equations for the Thermoelectric Effects

Given a pair of thermoelectric materials, $A$ and $B$, with each having a thermoelectric power $\alpha_A$ and $\alpha_B$,[42] the Seebeck coefficient is

$$\alpha = |\alpha_A| + |\alpha_B| \tag{54.97}$$

The Seebeck coefficient is the proportionality constant between the Seebeck voltage and the junction temperature with respect to some reference temperature

$$dE_s = \pm \alpha dT$$

and it is seen that

$$\alpha = \frac{dE_s}{dt}$$

The Peltier heat is proportional to the current flow and the proportionality constant is $\Pi$, the Peltier-voltage

$$q_p = \pm \Pi I \tag{54.98}$$

The Thomson heat is proportional to a temperature difference $dT$ and the proportionality constant is $\sigma$, the Thomson coefficient. With $dq_T = \pm \sigma I\, dt$, it is observed that $\sigma\, dT$ is a voltage and the Thomson voltage is defined by

$$E_T = \pm \int_{T_1}^{T_2} \sigma dT$$

Considerations of the second laws of thermodynamics and the Kirchhoff voltage laws show that the Peltier voltage is related to the Seebeck coefficient[42]

$$\Pi = \alpha T \tag{54.99}$$

and if the Seebeck coefficient is represented as a polynomial[42]

$$\alpha = a + bT + \cdots$$

then

$$\Pi = aT + bT^2 + \cdots$$

### Design Equations

In Fig. 54.13, which shows a pair of materials arranged as a thermoelectric cooler, there is a cold junction at $T_c$ and a hot junction at $T_h$. The materials possess a thermal conductivity $k$ and an electrical resistivity $\rho$. A voltage is provided so that a current $I$ flows through the cold junction from $B$ to $A$ and through the hot junction from $A$ to $B$. This current direction is selected to guarantee that $T_c < T_h$.

The net heat absorbed at the cold junction is the Peltier heat

$$q_p = \Pi T_c = \alpha I T_c \tag{54.100a}$$

minus one-half of the $I^2R$ loss (known as the Joule heat or Joule effect)

$$q_j = \tfrac{1}{2} I^2 R \tag{54.100b}$$

and minus the heat regained at the cold junction (known as the Fourier heat or Fourier effect) due to the temperature difference $\Delta T = T_h - T_c$

$$q_F = K\,\Delta T = K(T_h - T_c) \tag{54.100c}$$

Thus the net heat absorbed at the cold junction is

$$q = \alpha I T_c - \tfrac{1}{2} I^2 R - K\,\Delta T \tag{54.101}$$

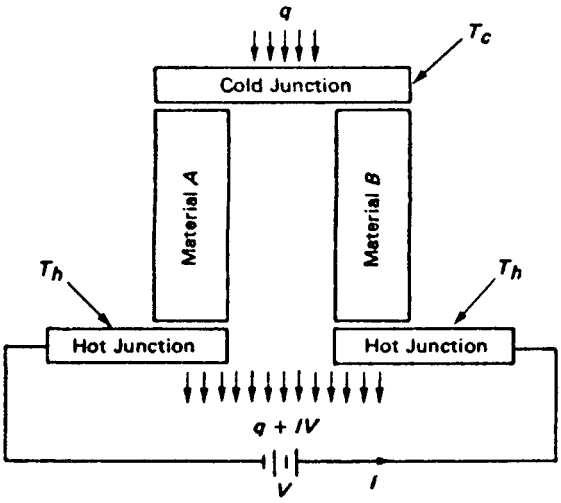


**Fig. 54.13** Thermoelectric cooler.

where the total resistance of the couple is the series resistance of material $A$ and material $B$ having areas $A_A$ and $A_B$, respectively (both have length $L$),

$$R = \left(\frac{\rho_A}{A_A} + \frac{\rho_B}{A_B}\right) L \tag{54.102}$$

and where the overall conductance $K$ is the parallel conductance of the elements $A$ and $B$:

$$K = \frac{1}{L}(k_A A_A + k_B A_B) \tag{54.103}$$

In order to power the device, a voltage equal to the sum of the Seebeck voltages at the hot and cold junctions plus the voltage necessary to overcome the resistance drop must be provided:

$$V = \alpha T_h - \alpha T_c + RI = \alpha\,\Delta T + RI$$

and the power is

$$P = VI = (\alpha\,\Delta T + RI)I \tag{54.104}$$

The coefficient of performance (COP) is the ratio of the net cooling effect to the power provided:

$$\text{COP} = \frac{q}{P} = \frac{\alpha T_c I - \frac{1}{2} I^2 R - K\,\Delta T}{\alpha \Delta T I + I^2 R} \tag{54.105}$$

### Optimizations

The maximum possible temperature differential $\Delta T = T_h - T_c$ will occur when there is no net heat absorbed at the cold junction:

$$\Delta T_m = \tfrac{1}{2} z T_c^2 \tag{54.106}$$

where $z$ is the figure of merit of the material

$$z = \frac{\alpha^2}{KR} \tag{54.107}$$

The current that yields the maximum amount of heat absorbed at the cold junction can be shown to be[42]

$$I = I_m = \frac{\alpha T_c}{R} \tag{54.108}$$

and the coefficient of performance in this case will be

$$\text{COP}_m = \frac{1 - \Delta T/\Delta T_m}{2(1 + \Delta T/T_c)} \tag{54.109}$$

The current that optimizes or maximizes the coefficient of performance can be shown to be

$$I_0 = \frac{\alpha \Delta T}{R[(1 + zT_a)^{1/2} - 1]} \tag{54.110}$$

where $T_a = \frac{1}{2}(T_h + T_c)$. In this case, the optimum coefficient of performance will be

$$\text{COP}_0 = \frac{T_c}{\Delta T}\left[\frac{\gamma - (T_h/T_c)}{\gamma + 1}\right] \tag{54.111}$$

where

$$\gamma = [1 + \tfrac{1}{2}z\,(T_h + T_c)]^{1/2} \tag{54.112}$$

### Analysis of Thermoelectric Coolers

In the event that a manufactured thermoelectric cooling module is being considered for a particular application, the designer will need to specify the number of junctions required. A detailed procedure for the selection of the number of junctions is as follows:

1. Design specifications
   (a) Total cooling load, $q_T$, $W$
   (b) cold-side temperature, $T_c$, °K
   (c) Hot-side temperature, $T_h$, °K
   (d) Cooler specifications
      i. Materials $A$ and $B$
      ii. $\alpha_A$ and $\alpha_B$, V/°C
      iii. $\rho_A$ and $\rho_B$, ohm · cm
      iv. $k_A$ and $k_B$, $W$/cm · °C
      v. $A_A$ and $A_B$, cm$^2$
      vi. $L$, cm
2. Cooler calculations
   (a) Establish $\alpha = |\alpha_A| + |\alpha_B|$
   (b) Calculate $R$ from Eq. (54.102)
   (c) Calculate $K$ from Eq. (54.103)
   (d) Form $\Delta T = T_h - T_c$, K or °C
   (e) Obtain $z$ from Eq. (54.107), 1/°C
3. For maximum heat pumping per couple
   (a) Calculate $I_m$ from Eq. (54.108), A
   (b) Calculate the heat absorbed by each couple $q$, from Eq. (54.101), W
   (c) Calculate $\Delta T_m$ from Eq. (54.106), K or °C
   (d) Determine $\text{COP}_m$ from Eq. (54.109)
   (e) The power required per couple will be $p = q/\text{COP}_m$, W
   (f) The heat rejected per couple will be $p + q$, W
   (g) The required number of couples will be $n = q_T/q$
   (h) The total power required will be $p_T = nP$, W
   (i) The total heat rejected will be $q_{RT} = nq_R$, W

3A. For optimum coefficient of performance
   (a) Determine $T_a = \frac{1}{2}(T_h + T_c)$, K
   (b) Calculate $I_0$ from Eq. (54.110), A
   (c) Calculate the heat absorbed by each couple, $q$, from Eq. (54.101), W
   (d) Determine $\gamma$ from Eq. (54.112)
   (e) Determine $\text{COP}_0$ from Eq. (54.111)
   (f) The power required per couple will be $P = q/\text{COP}_0$, W
   (g) The heat rejected per couple will be $q_R = P + q$, W
   (h) The required number of couples will be $n = q_T/q$

(i) The total power required will be $P_T = nP$, W
(j) The total heat rejected will be $q_{RT} = nq_R$, W

## REFERENCES


1. K. J. Negus, R. W. Franklin, and M. M. Yovanovich, "Thermal Modeling and Experimental Techniques for Microwave Bi-Polar Devices," *Proceedings of the Seventh Thermal and Temperature Symposium,*" San Diego, CA, 1989, pp. 63–72.
2. M. M. Yovanovich and V. W. Antonetti, "Application of Thermal Contact Resistance Theory to Electronic Packagès," in *Advances in Thermal Modeling of Electronic Components and Systems,* A. Bar-Cohen and A. D. Kraus (eds.), Hemisphere, New York, 1988, pp. 79–128.
3. *Handbook of Chemistry and Physics (CRC),* Chemical Rubber Co., Cleveland, OH, 1954.
4. W. Elenbaas, "Heat Dissipation of Parallel Plates by Free Convection," *Physica* **9**(1), 665–671 (1942).
5. J. R. Bodoia and J. F. Osterle, "The Development of Free Convection Between Heated Vertical Plates," *J. Heat Transfer* **84**, 40–44 (1964).
6. A. Bar-Cohen, "Fin Thickness for an Optimized Natural Convection Array of Rectangular Fins," *J. Heat Transfer* **101**, 564–566.
7. A. Bar-Cohen and W. M. Rohsenow, "Thermally Optimum Arrays of Cards and Fins in Natural Convection," *Trans IEEE Chart, CHMT-6,* 154–158.
8. E. M. Sparrow, J. E. Niethhammer, and A. Chaboki, "Heat Transfer and Pressure Drop Characteristics of Arrays of Rectangular Modules Encountered in Electronic Equipment," *Int. J. of Heat and Mass Transfer* **25**(7), 961–973 (1982).
9. R. A. Wirtz and P. Dykshoorn, "Heat Transfer from Arrays of Flatpacks in Channel Flow," *Proceedings of the Fourth Int. Electronic Packaging Society Conference,* New York, 1984, pp. 318–326.
10. S. B. Godsell, R. J. Dischler, and S. M. Westbrook, "Implementing a Packaging Strategy for High Performance Computers," *High Performance Systems,* 28–31 (January 1990).
11. A. D. Kraus and A. Bar-Cohen, *Design and Analysis of Heat Sinks,* Wiley, New York, 1995.
12. M. Jakob, *Heat Transfer,* Wiley, New York, 1949.
13. S. Globe and D. Dropkin, "Natural Convection Heat Transfer in Liquids Confined by Two Horizontal Plates and Heated from Below," *J. Heat Transfer, Series C* **81**, 24–28 (1959).
14. W. Mull and H. Rieher, "Der Warmeschutz von Luftschichten," *Gesundh-Ing. Beihefte* **28** (1930).
15. J. G. A. DeGraaf and E. F. M. von der Held, "The Relation Between the Heat Transfer and the Convection Phenomena in Enclosed Plane Air Layers," *Appl. Sci. Res., Sec. A* **3**, 393–410 (1953).
16. A. Bar-Cohen and W. M. Rohsenow, "Thermally Optimum Spacing of Vertical, Natural Convection Cooled, Parallel Plates," *J. Heat Transfer* **106**, 116–123 (1984).
17. S. W. Churchhill and R. A. Usagi, "A General Expression for the Correlation of Rates of Heat Transfer and Other Phenomena,," *AIChE J* **18**(6), 1121–1138 (1972).
18. N. Sobel, F. Landis, and W. K. Mueller, "Natural Convection Heat Transfer in Short Vertical Channels Including the Effect of Stagger," *Proceedings of the Third International Heat Transfer Conference,* Vol. 2, Chicago, IL, 1966, pp. 121–125.
19. W. Aung, L. S. Fletcher, and V. Sernas, "Developing Laminar Free Convection Between Vertical Flat Plates with Asymmetric Heating," *Int. J. Heat Mass Transfer* **15**, 2293–2308 (1972).
20. O. Miyatake, T. Fujii, M. Fujii, and H. Tanaka, "Natural Convection Heat Transfer Between Vertical Parallel Plates—One Plate with a Uniform Heat Flux and the Other Thermally Insulated," *Heat Transfer Japan Research* **4**, 25–33 (1973).
21. W. Aung, "Fully Developed Laminar Free Convection Between Vertical Flat Plates Heated Asymetrically," *Int. J. Heat Mass Transfer* **15**, 1577–1580 (1972).
22. W. H. McAdams, *Heat Transmission,* 3rd ed., McGraw-Hill, New York, 1954.
23. R. Hilpert, Warmeabgue von Geheizten Drähten and Rohren in Lufstrom, *Forsch, Ing-Wes* **4**, 215–224 (1933).
24. S. Whitaker, "Forced Convection Heat Transfer Correlations for Flow in Pipes, Past Flat Plates, Single Cylinders, Single Spheres and for Flow in Packed Beds and Tube Bundles," *AIChE Journal* **18**, 361–371 (1972).
25. F. Kreith, *Principles of Heat Transfer,* International Textbook Co., Scranton, PA, 1959.
26. A. P. Colburn, "A Method of Correlating Forced Convection Heat Transfer Data and a Comparison of Fluid Friction," *Trans AIChE* **29**, 174–210 (1933).
27. "Standards of the Tubular Exchanger Manufacturer's Association," New York, 1949.
28. W. Drexel, "Convection Cooling," *Sperry Engineering Review* **14**, 25–30 (December 1961).

**29.** W. Robinson and C. D. Jones, *The Design of Arrangements of Prismatic Components for Cross-flow Forced Air Cooling,* Ohio State University Research Foundation Report No. 47, Columbus, OH, 1955.

**30.** W. Robinson, L. S. Han, R. H. Essig, and C. F. Heddleson, *Heat Transfer and Pressure Drop Data for Circular Cylinders in Ducts and Various Arrangements,* Ohio State University Research Foundation Report No. 41, Columbus, OH, 1951.

**31.** E. N. Sieder and G. E. Tate, "Heat Transfer and Pressure Drop of Liquids in Tubes," *Ind. Eng. Chem.* **28**, 1429–1436 (1936).

**32.** H. Hausen, *Z VDI, Beih. Verfahrenstech.* **4**, 91–98 (1943).

**33.** A. L. London, "Air Coolers for High Power Vacuum Tubes," *Trans. IRE* **ED-1**, 9–26 (April, 1954).

**34.** K. A. Gardner, "Efficiency of Extended Surfaces," *Trans. ASME* **67**, 621–631 (1945).

**35.** W. M. Murray, "Heat Transfer Through an Annular Disc or Fin of Uniform Thickness," *J. Appl. Mech.* **5**, A78–A80 (1938).

**36.** D. Q. Kern and A. D. Kraus, *Extended Surface Heat Transfer,* McGraw-Hill, New York, 1972.

**37.** D. E. Briggs and E. H. Young, "Convection Heat Transfer and Pressure Drop of Air Flowing across Triangular Pitch Banks of Finned Tubes," *Chem. Eng. Prog. Symp. Ser.* **41**(59), 1–10 (1963).

**38.** A. D. Kraus, A. D. Snider, and L. F. Doty, "An Efficient Algorithm for Evaluating Arrays of Extended Surface," *J. Heat Transfer* **100**, 288–293 (1978).

**39.** A. D. Kraus, *Analysis and Evaluation of Extended Surface Thermal Systems,* Hemisphere, New York, 1982.

**40.** A. D. Kraus and A. D. Snider, "New Parametrizations for Heat Transfer in Fins and Spines," *J. Heat Transfer* **102**, 415–419 (1980).

**41.** W. M. Kays and A. L. London, *Compact Heat Exchangers,* 3rd ed., McGraw-Hill, New York, 1984.

**42.** A. D. Kraus and A. Bar-Cohen, *Thermal Analysis and Control of Electronic Equipment,* Hemisphere, New York, 1983.